Chemical Communications

COMMUNICATION

Facile meltPEGylation of Flame-made Luminescent Tb^{3+}-doped Yttrium Oxide Particles: Hemocompatibility, Cellular Uptake and Comparison to Silica

Received 00th January 20xx,
Accepted 00th January 20xx

DOI: 10.1039/x0xx00000x

www.rsc.org/

Kerda Keevend[a‡], Guido Panzarasa[b‡], Fabian H.L. Starsich[c], Martin Zeltner[d], Anastasia Spyrogianni[c], Elena Tsolaki[e], Giuseppino Fortunato[b], Sotiris E. Pratsinis[c], Sergio Bertazzo[e], Inge K. Herrmann[a,*]

Flame aerosol technology is a versatile method for scalable synthesis of nanoparticles. Since particles are produced and collected in a dry state, dispersibility and further functionalization could pose hurdles to their biomedical use. We report on a one-pot, scalable and robust procedure for the PEGylation of flame-made yttria and silica nanoparticles. We demonstrate improved colloidal stability, attenuated activation of blood coagulation and decreased uptake into phagocytic cells, all of which pave the way for facilitated biomedical use of flame-made oxide nanoparticles.

Flame aerosol technology is a versatile process that allows large scale production of high quality nanoparticles.[1, 2] Its broad use for decades further evidences the process robustness and applicability for synthesis of nanoparticles, even by industrial standards.[3] Spray combustion of solutions[4] has been employed for preparing a wide range of mono- and multicomponent nanoparticles at low cost and with high yields in commercial quantities.[5] It can be scaled up to a production rate of kg per hour[6] without significant alterations in material characteristics,[7] and specifically for biomedically relevant materials.[8, 9] In the recent years, flame-made particles with diverse compositions and architectures (including core/shell[10] and Janus shaped[11, 12] particles) have attracted increasing interest in the biomedical field. The good stoichiometric control and scalability of the process along with the sterility of the high temperature conditions make flame spray pyrolysis[4] an attractive method for synthesis[13] of nanoparticles for diagnostic[9] and therapeutic use.[14] While some applications are based on the incorporation of flame-made nanoparticles into polymeric matrices and composites,[15, 16] others rely on direct topical application of nanoparticles without any functionalization.[17] However, such fumed metal oxide nanoparticles can be damaging to cells.[18, 19] Especially flame-made silica and silica-rich materials have been shown to activate blood coagulation and lyse cellular membranes.[20, 21]

While surface modification of such nanoparticles can effectively attenuate the damaging effects,[22] stabilization and further functionalization of flame-made particles often is challenging. Among the different strategies available to modify the surface of nanoparticles, functionalization with poly(ethylene glycol) chains (PEGylation) is first choice, primarily because the hydrophilic and flexible PEG chains disperse well in physiological media due to steric repulsion.[23] Additionally, it has been shown that surface PEGylation attenuates non-specific protein adsorption,[24] prolongs blood circulation times and reduces uptake into phagocytic cells.[22] While it is relatively straightforward to achieve high surface grafting densities with small molecules (such as silanes),[25] it generally remains challenging to achieve high PEG-chain grafting densities on the nanoparticle surface. A promising method for *in situ* functionalization of flame-made titania nanoparticles with hydrophobic moieties that were thermally stable up to 300°C in air was reported,[26] however, its applicability for PEG-based silanes has yet to be demonstrated. Various strategies have been developed for PEGylation of metal oxide nanoparticles.[27] Most of them involve the use of PEG derivatives with reactive chain ends (such as silanes[28] and phosphonates[29-31]) or sophisticated surface polymerization reactions of PEG-like monomers. Other methods include Atom Transfer Radical Polymerization (ATRP)[32] and reversible addition-fragmentation chain transfer (RAFT)-based approaches.[33] However, there is a need for more straightforward, user-friendly and universally applicable alternatives not relying on expert know-how or expensive reactive-group terminated PEG moieties.

Melt grafting was developed in the 1980s as a straightforward route for the hydrophobization of sol-gel (Stöber) silica particles. In the original protocols, silica particles dispersed in a long-chain alcohol (such as stearyl alcohol) were heated to 180-200 °C (usually for 1 to 3 hrs) to promote the esterification reaction between the surface silanols and the alcohol -OH groups, through the formation of Si–O–C bonds.[34] After cooling, the particles were re-dispersible in non-

[a] *Particles 4D, Particles Biology Interactions, Department Materials Meet Life, Swiss Federal Laboratories for Materials Science and Technology (Empa), Lerchenfeldstrasse 5, CH-9014, St. Gallen, Switzerland.*
[b] *Biomimetic Membranes and Textiles, Department Materials Meet Life, Swiss Federal Laboratories for Materials Science and Technology (Empa), Lerchenfeldstrasse 5, CH-9014, St. Gallen, Switzerland.*
[c] *Particle Technology Laboratory, Institute of Process Engineering, Department of Mechanical and Process Engineering, ETH Zurich, Sonneggstrasse 3, CH-8092 Zurich, Switzerland.*
[d] *Functional Materials Laboratory, Institute for Chemical and Bioengineering, Department of Chemistry and Applied Biosciences, ETH Zurich, Vladimir-Prelog-Weg 1, CH-8093 Zurich, Switzerland.*
[e] *Departments of Medical Physics and Biomedical Engineering, University College London (UCL), Malet Place Engineering Building, London, WC1E 6BT, United Kingdom.*
[‡] contributed equally as first authors.
Electronic Supplementary Information (ESI) available: Experimental (S1-S3). Particle characterization (Fig. S1). XPS and XRD (Fig. S2), DLS data (Figs. S3 and S4). RF/D values (Tab. S1) See DOI: 10.1039/x0xx00000x

polar organic solvents.[35] However, interest for this approach was lost when hydrophobic silanes started to become widely available.[36] More recently, melt-grafting protocols started again to attract attention due to their simplicity. For example, an approach for meltPEGylation of iron oxide particles has been recently reported,[23] which however, makes use of particles first functionalized with nitrodopamine or nitrodopamine-PEG chains and thus does not constitute a one-pot approach analogous to the historical method.

Here, we present an effective, robust and straightforward route to obtain stabilized colloids of flame-made nanoparticles using low cost monomethylether-terminated PEG. We demonstrate the versatility of the meltPEGylation protocol by applying it to two different oxide nanoparticles, luminescent terbium-doped yttria (Y_2O_3:Tb^{3+}) and silica (SiO_2). Luminescent Y_2O_3:Tb^{3+} nanoparticles were included as a biomedically-promising material with prospective applications in labelling of cancerous cells.[37] Flame-made SiO_2 is a commercially relevant and well-known material with comparatively poor cyto-[15] and hemocompatibility.[17, 21] In addition, silica has been historically important in the development of melt-grafting protocols,[34] and is thus used for benchmarking. The obtained PEG grafting densities are compared to those achieved by simple PEG physisorption and PEG-silane grafting. To assess the feasibility of meltPEGylated flame-made metal oxide nanoparticles for biomedical applications, their properties such as colloidal stability over time, cytocompatibility, activation of the blood coagulation cascade and uptake into phagocytes were investigated.

Both Y_2O_3:Tb^{3+} and SiO_2 nanoparticles were prepared by flame spray pyrolysis following previously reported protocols.[21, 38] In brief, metal organic precursor solutions, containing the desired stoichiometric amounts of elements, were prepared and combusted. Particles were collected on a filter downstream of the flame and subsequently subjected to physicochemical characterization. The specific surface area measured by N_2 adsorption (BET method) was 230 m^2/g for silica and 71 m^2/g for Tb^{3+}-doped yttria nanoparticles. The corresponding average primary particle sizes (d_{BET}) were 10 nm for SiO_2 and 16 nm for Y_2O_3:Tb^{3+}, in line with values reported in literature obtained under comparable process conditions.[21, 38] Nanoparticle morphology was studied by transmission electron microscopy (TEM) and crystallinity by X-ray powder diffraction (XRD) (**Figures 1a,b** and **S1**). Y_2O_3:Tb^{3+} nanoparticles are monoclinic and highly crystalline, while silica is amorphous, which is in good agreement with the literature.[21,31] The carbon content of as-prepared nanoparticles prior to surface modification determined by elemental analysis (CHN analysis) was < 0.1 wt%. The as-prepared materials were then subjected to two different PEGylation protocols, namely meltPEGylation and PEG physisorption. For meltPEGylation, a procedure similar to the historical method was used.[34] In short, as-prepared nanoparticles were ground in a mortar together with poly(ethylene glycol) monomethyl ether. PEG monomethyl ether was chosen to avoid cross-linking. After mixing with ethanol and subsequent solvent evaporation, the solid was heated to 200 °C under inert atmosphere and nanoparticles were washed repeatedly with solvents (see **ESI** for detailed methods). For the PEG physisorption protocol, the nanoparticles were directly dispersed in solvents containing dissolved PEG and washed afterwards. The grafting densities calculated from the PEG loading and the BET surface were distinct for the different functionalization routes (**Table 1**: CHN analysis). The highest grafting densities (1.2 chains per nm^2 for Y_2O_3:Tb^{3+} and 0.8 chains per nm^2 for SiO_2) were found for particles functionalized by the meltPEGylation route using PEG350. For Y_2O_3:Tb^{3+}, a 50% increase in PEG loading using meltPEGylation compared to physisorption was found for all three molecular weights studied (350, 1900 and 5000 Da). For comparison, surface grafting densities for functionalization with commercially available PEG-silanes following the protocol described by Lucky *et al.*[39] were included in **Table 1**. Grafting densities obtained by the meltPEGylation route are comparable to reported maximum PEG densities on silica (0.24-2.3 chains per nm^2)[40] and iron oxide (0.5-3 chains per nm^2).[23] Importantly, meltPEGylation can give access to a brush-like conformation of PEG. The average distance D between neighboring PEG chains on particle surface determines the structural conformation of the surface-attached PEG chains and thus its shielding effectiveness. If D is greater than the Flory radius R_F, that, is, if $R_F/D \leq 1$, neighboring PEG chains will not overlap and are said to be in a "mushroom" conformational regime. However, as the surface PEG density increases such that adjacent PEG chains overlap, that is, if $R_F/D > 1$, PEG chains are forced to stretch away from the particle surface forming a "brush" layer. It is generally believed that surface

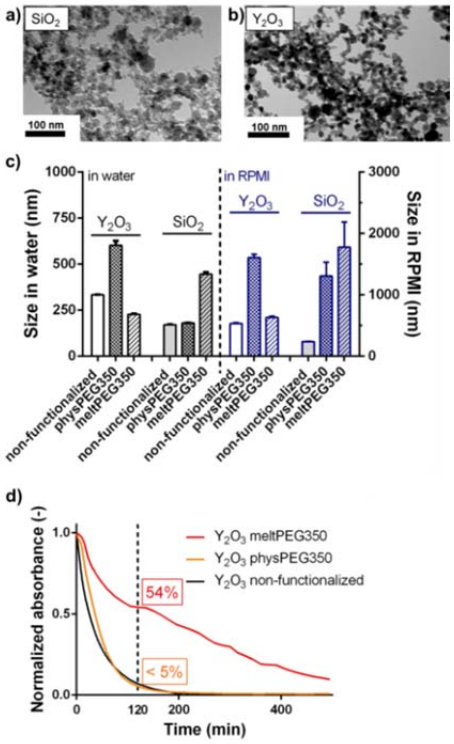

Figure 1: *Transmission electron micrographs (TEM) of SiO_2 (a) and Y_2O_3:Tb^{3+} (b). Dynamic light scattering (DLS) measurements for Y_2O_3:Tb^{3+} and SiO_2 nanoparticle suspensions in water (left) and serum-containing medium used for cell culture (right) before and after PEGylation (physisorption vs. meltPEGylation) (c). Particle sedimentation measured by UV-Vis absorption at 350 nm over 8 hours for Y_2O_3:Tb^{3+} nanoparticles (d).*

Table 1: *PEG grafting densities for the different functionalization routes.*

	PEG content (wt% C)			Grafting density (chains/nm^2)			meltPEG chain density relative to SiO_2 (-)
	Phys	*Melt*	*Silane*	*Phys*	*Melt*	*Silane*	
Y_2O_3PEG350	3.32	5	1.32	0.8	1.2	0.3	1.5 ×
Y_2O_3PEG1900	3.07	4.06	-	0.14	0.18	-	2.6 ×
Y_2O_3PEG5000	2.78	3.5	1.83	0.04	0.06	0.03	1.5 ×
SiO_2PEG350	0.32	10.52	1.56	0.02	0.8	0.11	1 ×
SiO_2PEG1900	1.06	4.73	-	0.013	0.07	-	1 ×
SiO_2PEG5000	1.99	7.95	2.25	0.01	0.04	0.011	1 ×

PEG densities in the mushroom-to-brush transition state are required to offer optimal performance.[41] The results obtained for Y_2O_3:Tb^{3+} suggest that while PEG physisorption leads only to a "mushroom" state, meltPEGylation can give access to a "brush" layer (**ESI, Table S1**). Densities are likely to vary between different particles due to different compositions and availabilities of surface hydroxyl groups.

The phase and the luminescent properties of the Y_2O_3:Tb^{3+} particles remained unaltered after PEGylation (**ESI, Figure S1 and S2**). Fourier transform infrared spectroscopy further confirmed the presence of PEG on both Y_2O_3:Tb^{3+} and SiO_2 nanoparticles (**ESI, Figure S1**). X-ray photoelectron spectroscopy of meltPEG on silica showed a small chemical shift towards Si-O-C, however, the Si-O-C and O-Si-O peak show significant overlap (**ESI, Figure S2**). Following PEGylation, colloidal size and particle sedimentation were measured by DLS and ultraviolet-visible (UV-Vis) spectroscopy using particle suspensions in water and cell culture medium (**Figures 1b** and **S3 (ESI)**). From DLS measurements in water, it became evident that meltPEGylated yttria nanoparticles have smaller hydrodynamic diameters compared to non-functionalized and physisorbed PEG nanoparticles (**Figure 1c**). Particles with the shortest polymer chain length (*i.e.* 350 Da) have the smallest hydrodynamic size (**ESI, Figure S3a**) and the highest grafting densities. Therefore, nanoparticles functionalized with PEG350 were selected for further investigations. The polydispersity indices (PDI) (see **Figure S3a**) were generally smaller for meltPEGylated particles compared to the values observed for physisorbed PEG particles. In cell culture medium, meltPEGylated Y_2O_3:Tb^{3+} nanoparticles remained much smaller compared to physisorbed PEG nanoparticles (see **ESI Figure S3 b-f** for raw data). While hydrodynamic sizes of PEGylated silica nanoparticles were significantly larger in cell culture medium compared to water, non-functionalized silica nanoparticles remained remarkably small in serum-containing medium. This is in agreement with previous reports showing high stability of non-functionalized silica at similar concentrations in cell culture medium over time.[42] . Interestingly, when dispersions were measured immediately after preparation, hydrodynamic sizes were comparable for all nanoparticles (in both water and medium) and below 300 nm (see **ESI, Figure S4**). The differences in long-term stability indicate that the PEG chain length and purification protocols may require optimization for different metal oxides and environments (buffers, protein-rich solutions, *etc*). To further characterize the colloidal stability of the Y_2O_3:Tb^{3+} suspensions, sedimentation over time was measured according to procedures described by Spyrogianni *et al.*[42] Sedimentation was monitored in a 3 mm deep suspension layer over 8 hrs by UV-Vis spectroscopy (**Figure 1d**). Non-functionalized Y_2O_3:Tb^{3+} nanoparticles show fast sedimentation within the first 30 minutes, similar to those functionalized by the physisorption route. For non-functionalized and physisorbed PEG, the dispersion reached < 5% of its initial absorbance after 2 hours, whereas for particles prepared by the meltPEGylation route, the absorbance was still > 50% of the initial value after 2 hrs. The sedimentation kinetics illustrates the improved colloidal stability of meltPEGylated particles compared to non-functionalized nanoparticles and those functionalized with PEG physisorption.

Next, we assessed the influence of the different PEGylation routes on the biological fate of the nanoparticles. Cytocompatibility was assessed in a membrane integrity assay in a dose-dependent manner on human THP-1 monocytes. Since particle size is an important factor in cytotoxicity studies,[43] that determines also particle settling rate,[20] a suspension culture was chosen, accounting for potentially different sedimentation properties. Lactate dehydrogenase (LDH) release, as a surrogate marker for membrane damage, was studied in monocytes (in suspension) for Y_2O_3:Tb^{3+} and SiO_2 nanoparticles in

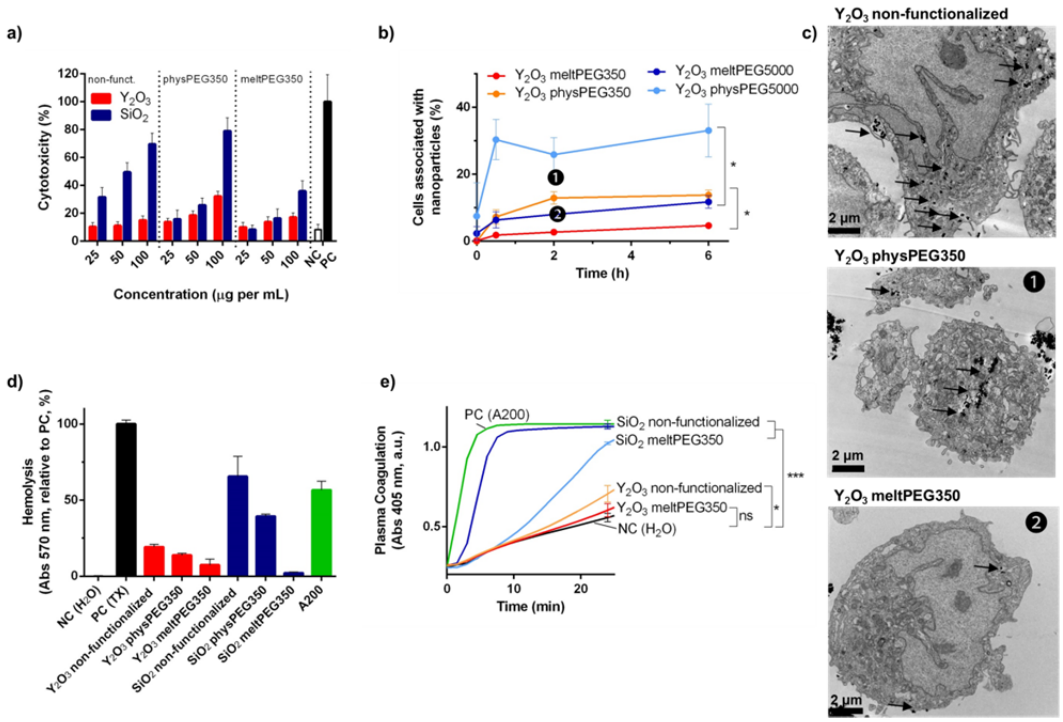

Figure 2: *Particle induced lactate dehydrogenase (LDH) release in THP-1 monocytes after exposure to non-functionalized, physisorbed PEG and meltPEGylated yttria and silica nanoparticles in serum-containing conditions for 24 hours (a). Cellular uptake measured by the number of cells associated with nanoparticles in flow cytometry for different PEGylation protocols and chain lengths (b). Corresponding transmission electron micrographs of cells incubated with different particles (2 hrs time point) (c). Hemolysis in response to particle exposure (100 µg per mL for 3 hours) (d). Plasma coagulation measured at 405 nm (fibrin polymerization) comparing native plasma to plasma samples pre-exposed to nanoparticles. (e). Aerosil200 was used as positive control (PC), H_2O (vehicle) served as negative control (NC). Experiments were carried out at least three times (N ≥ 3). * indicates p < 0.05 and *** indicates p < 0.001.*

serum-containing conditions (**Figure 2a**). Generally, silica nanoparticles led to higher LDH release at equivalent doses compared to Y_2O_3:Tb^{3+}. All yttria nanoparticles displayed low toxicity before and after functionalization, while silica exhibited relevant membrane damage potential. Silica particles functionalized with physisorbed PEG showed cytotoxicity similar to as-prepared nanoparticles, whereas cells exposed to meltPEGylated silica nanoparticles led to significantly lower LDH release.

To investigate whether higher PEG chain density and therefore reduced protein interaction could also translate into altered uptake into phagocytic cells, we assessed the uptake into human monocytes as a function of time (**Figure 2b**). By means of flow cytometry,[44, 45] we compared the fraction of cells associated with (*i.e.* membrane-bound or uptaken) particles for Y_2O_3:Tb^{3+} nanoparticles functionalized with physisorbed PEG and by meltPEGylation. Cell-free controls were measured to exclude interference from particle aggregates. Time-dependent shifts in the side-scattering (SSC) signal indicated a more rapid association and internalization of particles carrying physisorbed PEG compared to meltPEGylated Y_2O_3:Tb^{3+}. These results were also confirmed for nanoparticles functionalized with 5000 Da PEG chains. The lower association of nanoparticles with cells was further verified by transmission electron microscopy (**Figure 2c**). Transmission electron micrographs were recorded for cell samples incubated with the different nanoparticles for 2 hours. For non-functionalized and physisorbed PEG samples, a higher number of intracellular particle agglomerates can be found compared to meltPEGylated samples. In meltPEGylated samples, very few particles are localized intracellularly. A few particle agglomerates associated with the outer cell membrane can be observed, indicating a delayed particle uptake compared to the non-functionalized and physisorbed PEG samples. The flow cytometry data (**Figure 2b**) together with the transmission electron micrographs (**Figure 2c**) suggest a delayed particle uptake into monocytes for meltPEGylated particles, which may translate into altered biodistribution. Hydrodynamic particle size (d_H) and the stealth properties of the PEG are main parameters governing particle uptake kinetics, especially into the liver ($d_H > 100$ nm) and spleen ($d_H > 200$ nm).[46]

If nanoparticles are intended for intravascular application, hemocompatibility is of utmost importance. We therefore assessed the effect of as-prepared and PEGylated nanoparticles on red blood cells (particle concentration of 0.1 mg mL^{-1}) in a hemolysis assay (**Figure 2d**). As-prepared silica nanoparticles were highly hemolytic with hemolysis reaching levels > 50% relative to positive control, similar to commercially available fumed silica (Aerosil200). The high hemolytic activity of flame made and fumed silica is in good agreement with previous studies reporting hemolytic properties for different silicas,[47] including Aerosil300.[48] Surface PEGylation significantly decreased the hemolytic activity (Spearman's rho: -0.95, $p < 0.001$ (two-tailed)). This effect was most pronounced for meltPEG350, where hemolysis was comparable to untreated control (< 5%). Compared to silica, Y_2O_3:Tb^{3+} was significantly less hemolytic, and again the hemolytic potential was diminished as a function of PEG grafting density (Spearman's rho: -0.94, $p < 0.001$ (two-tailed)). Apart from hemolysis, the activation of the blood coagulation cascade is one of the most critical issues related to intravascular application. It is well known that metal oxides, and particularly silica nanoparticles, promote plasma coagulation.[49] Indeed, non-functionalized silica led to a significant activation of the plasma coagulation cascade (**Figure 2e**), in good agreement with previous reports.[17, 50] Non-functionalized yttria was much less procoagulant in comparison to silica but still led to slightly increased fibrin polymerization compared to negative control. Importantly, both meltPEGylated Y_2O_3:Tb^{3+} and SiO_2 nanoparticles showed attenuation of the procoagulant effect observed for non-functionalized nanoparticles. For meltPEGylated Y_2O_3:Tb^{3+}, values were even in the range of the negative control.

The study demonstrates, for the first time to our knowledge, direct melt-grafting of readily available, monomethoxy-terminated PEG on a metal oxide other than silica. The results illustrate the potential of solvent-free meltPEGylation as an elegant (one-pot), robust and straightforward route to achieve high PEG grafting density on flame made yttria and silica nanoparticles. MeltPEGylation significantly improves colloidal stability, reduces procoagulant activity and uptake by phagocytic cells, and hence facilitates biomedical use of flame-made nanopowders.

Conflicts of interest There are no conflicts to declare**.**

Notes and references

1. W. Y. Teoh, R. Amal and L. Madler, *Nanoscale*, 2010, **2**, 1324-1347.
2. R. Strobel and S. E. Pratsinis, *Journal of Materials Chemistry*, 2007, **17**, 4743-4756.
3. S. E. Pratsinis, *Progress in Energy and Combustion Science*, 1998, **24**, 197-219.
4. L. Mädler and S. E. Pratsinis, *Journal of the American Ceramic Society*, 2002, **85**, 1713-1718.
5. E. K. Athanassiou, R. N. Grass and W. J. Stark, *Aerosol Science and Technology*, 2010, **44**, 161-172.
6. A. J. Gröhn, S. E. Pratsinis, A. Sánchez-Ferrer, R. Mezzenga and K. Wegner, *Industrial & Engineering Chemistry Research*, 2014, **53**, 10734-10742.
7. R. Mueller, L. Mädler and S. E. Pratsinis, *Chemical Engineering Science*, 2003, **58**, 1969-1976.
8. J. H. Byeon, *Scientific Reports*, 2016, **6**, 35104.
9. F. H. L. Starsich, G. A. Sotiriou, M. C. Wurnig, C. Eberhardt, A. M. Hirt, A. Boss and S. E. Pratsinis, *Advanced Healthcare Materials*, 2016, **5**, 2698-2706.
10. A. Teleki, M. Suter, P. R. Kidambi, O. Ergeneman, F. Krumeich, B. J. Nelson and S. E. Pratsinis, *Chemistry of Materials*, 2009, **21**, 2094-2100.
11. G. A. Sotiriou, A. M. Hirt, P.-Y. Lozach, A. Teleki, F. Krumeich and S. E. Pratsinis, *Chemistry of Materials*, 2011, **23**, 1985-1992.
12. S. H. Choi and Y. C. Kang, *Nanoscale*, 2013, **5**, 4662-4668.
13. N. Desai, *The AAPS Journal*, 2012, **14**, 282-295.
14. G. A. Sotiriou, F. Starsich, A. Dasargyri, M. C. Wurnig, F. Krumeich, A. Boss, J. C. Leroux and S. E. Pratsinis, *Advanced Functional Materials*, 2014, **24**, 2818-2827.
15. A. Camenzind, W. R. Caseri and S. E. Pratsinis, *Nano Today*, 2010, **5**, 48-65.
16. N. Hild, P. N. Tawakoli, J. G. Halter, B. Sauer, W. Buchalla, W. J. Stark and D. Mohn, *Acta Biomaterialia*, 2013, **9**, 9118-9125.
17. M. T. Matter, F. Starsich, M. Galli, M. Hilber, A. A. Schlegel, S. Bertazzo, S. E. Pratsinis and I. K. Herrmann, *Nanoscale*, 2017, **9**, 8418-8426.
18. A. Liberman, N. Mendez, W. C. Trogler and A. C. Kummel, *Surface science reports*, 2014, **69**, 132-158.
19. H. Zhang, D. R. Dunphy, X. Jiang, H. Meng, B. Sun, D. Tarn, M. Xue, X. Wang, S. Lin, Z. Ji, R. Li, F. L. Garcia, J. Yang, M. L. Kirk, T. Xia, J. I. Zink, A. Nel and C. J. Brinker, *Journal of the American Chemical Society*, 2012, **134**, 15790-15804.
20. A. Spyrogianni, G. A. Sotiriou, D. Brambilla, J.-C. Leroux and S. E. Pratsinis, *Journal of Aerosol Science*, 2017, **108**, 56-66.
21. A. Spyrogianni, I. K. Herrmann, K. Keevend, S. E. Pratsinis and K. Wegner, *Journal of Colloid and Interface Science*, 2017, **507**, 95-106.
22. X. P. Duan and Y. P. Li, *Small*, 2013, **9**, 1521-1532.
23. R. Zirbs, A. Lassenberger, I. Vonderhaid, S. Kurzhals and E. Reimhult, *Nanoscale*, 2015, **7**, 11216-11225.
24. S. D. Tavano R, Reddi E, Kos J, Rojnik M, Kocbek P, Iratni S, Scheglmann D, Colucci M, Echevarria IM, Selvestrel F, Mancin F, Papini E., *Nanomedicine*, 2010, **5**, 881-896.
25. Y. Maidenberg, S. Zhang, K. Luo, N. Akhavein and J. T. Koberstein, *Langmuir*, 2013, **29**, 11959-11965.
26. A. Teleki, N. Bjelobrk and S. E. Pratsinis, *Langmuir*, 2010, **26**, 5815-5822.
27. A. S. Karakoti, S. Das, S. Thevuthasan and S. Seal, *Angewandte Chemie International Edition*, 2011, **50**, 1980-1994.
28. C. Barrera, A. P. Herrera and C. Rinaldi, *Journal of Colloid and Interface Science*, 2009, **329**, 107-113.
29. J.-C. Boyer, M.-P. Manseau, J. I. Murray and F. C. J. M. van Veggel, *Langmuir*, 2010, **26**, 1157-1164.
30. L. Qi, J. Fresnais, P. Muller, O. Theodoly, J. F. Berret and J. P. Chapel, *Langmuir*, 2012, **28**, 11448-11456.

31. C. A. Traina and J. Schwartz, *Langmuir*, 2007, **23**, 9158-9161.
32. W. Li, Y. Xu, Y. Zhou, W. Ma, S. Wang and Y. Dai, *Nanoscale Research Letters*, 2012, **7**, 485-485.
33. M. Ma, S. Zheng, H. Chen, M. Yao, K. Zhang, X. Jia, J. Mou, H. Xu, R. Wu and J. Shi, *Journal of Materials Chemistry B*, 2014, **2**, 5828-5836.
34. C. C. Ballard, E. C. Broge, R. K. Iler, D. S. S. John and J. R. McWhorter, *The Journal of Physical Chemistry*, 1961, **65**, 20-25.
35. A. K. Van Helden, J. W. Jansen and A. Vrij, *Journal of Colloid and Interface Science*, 1981, **81**, 354-368.
36. A. van Blaaderen and A. Vrij, *Journal of Colloid and Interface Science*, 1993, **156**, 1-18.
37. G. A. Sotiriou, D. Franco, D. Poulikakos and A. Ferrari, *ACS Nano*, 2012, **6**, 3888-3897.
38. G. A. Sotiriou, M. Schneider and S. E. Pratsinis, *The Journal of Physical Chemistry C*, 2011, **115**, 1084-1089.
39. S. S. Lucky, N. Muhammad Idris, Z. Li, K. Huang, K. C. Soo and Y. Zhang, *ACS Nano*, 2015, **9**, 191-205.
40. Y. Shui, Y. Su, X. Kuang, W. Zhao, Y. Cai and D. Wang, *Polymer International*, 2017, **66**, 1395-1401.
41. J. S. Suk, Q. Xu, N. Kim, J. Hanes and L. M. Ensign, *Advanced Drug Delivery Reviews*, 2016, **99**, 28-51.
42. A. Spyrogianni, I. K. Herrmann, M. S. Lucas, J.-C. Leroux and G. A. Sotiriou, *Nanomedicine*, 2016, **11**, 2483-2496.
43. I.-Y. Kim, E. Joachim, H. Choi and K. Kim, *Nanomedicine: Nanotechnology, Biology and Medicine*, 2015, **11**, 1407-1416.
44. R. M. Zucker, E. J. Massaro, K. M. Sanders, L. L. Degn and W. K. Boyes, *Cytometry Part A*, 2010, **77A**, 677-685.
45. Y. Ibuki and T. Toyooka, in *Nanotoxicity: Methods and Protocols*, ed. J. Reineke, Humana Press, Totowa, NJ, 2012, pp. 157-166.
46. H. Arami, A. Khandhar, D. Liggitt and K. M. Krishnan, *Chemical Society Reviews*, 2015, **44**, 8576-8607.
47. C. Pavan, M. Tomatis, M. Ghiazza, V. Rabolli, V. Bolis, D. Lison and B. Fubini, *Chemical Research in Toxicology*, 2013, **26**, 1188-1198.
48. B. I. Gerashchenko, V. M. Gun'ko, I. I. Gerashchenko, I. F. Mironyuk, R. Leboda and H. Hosoya, *Cytometry*, 2002, **49**, 56-61.
49. J. Margolis, *Autralian Journal of Experimental Biology and Medicine*, 1961, **39**, 249-258.
50. L. Bircher, O. M. Theusinger, S. Locher, P. Eugster, B. Roth-Z'graggen, C. M. Schumacher, J. D. Studt, W. J. Stark, B. Beck-Schimmer and I. K. Herrmann, *Journal of Materials Chemistry B*, 2014, **2**, 3753-3758.